Large-scale parallel electric fields and return currents in a global simulation model

H. Arnold (iD), J. F. Drake (iD), M. Swisdak (iD), and J. Dahlin (iD)

View Online   Export Citation   CrossMark

Large-scale parallel electric fields and return currents in a global simulation model

H. Arnold,[1] (ID) J. F. Drake,[1] (ID) M. Swisdak,[1] (ID) and J. Dahlin[2] (ID)

AFFILIATIONS

[1]IREAP, University of Maryland, College Park, Maryland 20742–3511, USA
[2]NASA Goddard Space Flight Center, Greenbelt, Maryland 20771, USA

ABSTRACT

A new computational model, *kglobal*, is being developed to explore energetic electron production via magnetic reconnection in macroscale systems. The model is based on the discovery that the production of energetic electrons during reconnection is controlled by Fermi reflection in large-scale magnetic fields and not by parallel electric fields localized in kinetic scale boundary layers. Thus, the model eliminates these boundary layers. However, although the parallel electric fields that develop around the magnetic x-line and associated separatrices are not important in producing energetic electrons, there is a large scale electric field that kickstarts the heating of low-energy electrons and drives the cold-electron return current that accompanies escaping energetic electrons in open systems. This macroscale electric field is produced by magnetic-field-aligned gradients in the electron pressure. We have upgraded *kglobal* to include this large-scale electric field while maintaining energy conservation. The new model is tested by exploring the dynamics of electron acoustic modes which develop as a consequence of the presence of two electron species: hot kinetic and cold fluid electrons. Remarkably, the damping of electron acoustic modes is accurately captured by *kglobal*. Additionally, it has been established that *kglobal* correctly describes the dynamics of the interaction of the parallel electric field with escaping hot electrons through benchmarking simulations with the Particle-In-Cell code *p3d*.

I. INTRODUCTION

Solar flares convert magnetic energy into particle energy in the solar corona via magnetic reconnection.[16,17,32] From observations, we know that a significant fraction of the released energy during the reconnection event can go into accelerating energetic electrons, which form a suprathermal tail that takes the form of a power law distribution.[16,18,26] The plasma pressure from these nonthermal particles can be comparable to the pressure of the ambient magnetic field.[27,38] Further, using observations from the Wind spacecraft in the distant magnetotail, Øieroset *et al.*[37] found energetic electrons in a broad region around the x-line rather than in narrow boundary layers that would be expected in laminar 2D reconnection models.[6,8] Additionally, observations from the Reuven Ramaty High Energy Solar Spectroscopic Imager (RHESSI) and the Atmospheric Imaging Assembly on the Solar Dynamic Observatory, Krucker and Battaglia[28] revealed that a large fraction of the electron population in the above-the-loop-top source was energized to suprathermal energies. Multiple x-line reconnection can potentially describe both the diffuse distribution of energetic electrons seen in the Øieroset *et al.*[37] and Krucker and Battaglia[28] papers, and the large number of energetic electrons seen in flares.[18,36] This is because multiple x-line reconnection in 3D is turbulent and enables electrons to undergo acceleration in a much

larger volume than in a 2D system.[6] Additionally, it is now well known that current sheets can spawn multiple, volume-filling x-lines in three-dimensional systems in the presence of a guide field.[4,6,7,9] This behavior does not take place in antiparallel reconnection, even in a 3D system.[6]

In the past, simulations that study flares have been based on Particle-In-Cell (PIC) codes, magnetohydrodynamic (MHD) codes, or some combination thereof such as hybrid codes or MHD codes with an embedded PIC region.[21] However, explicit PIC models require that kinetic scales such as the Debye length be resolved. The Debye length is typically less than a centimeter in the solar corona yet the size of the flare itself can be up to ten orders of magnitude larger, a typical size being 10^4 km. Thus, using a PIC code to fully model a solar flare is computationally impossible. An MHD model, on the other hand, is not constrained by the need to resolve kinetic scales. However, since there are no particles in an MHD model, studying particle acceleration is not possible except by exploring the motion of test particles. While test particles can illuminate certain aspects of particle acceleration in solar flares, such as the primary mechanisms responsible for acceleration, there is no feedback of the energetic particles on the fields.[22] The particle energy can therefore run away. An embedded PIC code is an alternative but, since the energy release volume in flares is large and

the region the particles are accelerated is also broadly distributed, the separation of scales problem still exists. There are two dominant mechanisms that are responsible for particle heating and acceleration in magnetic reconnection: direct acceleration from parallel electric fields in diffusion regions and along magnetic separatrices,[2,42] and Fermi acceleration. Of these two, the latter is large scale and does not require resolving kinetic scales. Additionally, it has been recently proposed that Fermi acceleration, which occurs on macroscale, is what drives nonthermal particles and hence contributes to particle energization, rather than exclusively contributing to heating.[1,5,10,11,24,30,31] Thus, we are developing a new computational model, *kglobal*, which takes advantage of this discovery to order out all kinetic scales that must be resolved in PIC codes and conserves energy by particle feedback on the fields.[12] This model not only has an MHD backbone but also includes self-consistent feedback from particle electrons.

The process of magnetic reconnection leads to the formation of bent field lines whose tension drives an exhaust traveling at the upstream Alfvén speed.[34] Particles stream in along these bent, reconnected field lines which act like a moving wall and thus "kick" the particles which then increase in speed by twice the Alfvén speed.[10] However, it is known that a large-scale parallel electric field (not localized in boundary layers) facilitates this process by confining electrons within the reconnection exhaust such that they undergo multiple Fermi kicks.[13–15,25] Thus, it is of interest to include this large scale parallel electric field in our model to properly model the energy gain of low energy electrons. This potential is not, however, important to the dynamics of very energetic electrons. This field arises from parallel gradients in the electron pressure and points away from the current sheet in the reconnection exhaust. In an open system, it then drives a return current of cold electrons, which balances the current associated with escaping hot electrons to maintain zero net parallel current. We have updated the computational model *kglobal* to include the large scale electric field and present the results of testing herein. See the Appendix for a calculation of the parallel electric field and the exploration of energy conservation when this field is included.

A. The *kglobal* model with $E_\parallel$

Since the parallel electric fields that develop in kinetic scale boundary layers[8,39] are ineffective drivers of energetic electrons during reconnection,[3,5,6] we have formulated a model in which all kinetic scale boundary layers are eliminated.[12] This new model includes the key physics necessary to produce high energy particles without having to resolve kinetic scales. We do this by representing hot electrons as particles and cold electrons and ions as an MHD fluid. The hot electrons are evolved using the guiding center equations and they feedback on the fluid through their gyrotropic pressure tensor in the ion momentum equation. The electric and magnetic fields are evolved in the usual way from the MHD fluid. Drake *et al.*[12] presented in detail the derivation of this model. Crucially, this model conserves energy, which prevents the electron energy from running away. The dominant feedback is through the development of pressure anisotropy of the energetic electrons—a strong increase in the parallel electron pressure weakens the magnetic tension that drives reconnection, thereby throttling magnetic energy release. MHD codes are able to achieve normalized rates of reconnection that are on the order of 0.01 through the formation of multiple plasmoids. This rate is smaller than typical rates from PIC simulations.[35,40] However, through the introduction of

artificial resistivity and hyperviscosity, fast rates of reconnection can be achieved in the MHD model.[41] Care must be taken; however, that artificial dissipation does not suppress multiple x-line reconnection, which is required to produce a nonthermal particle spectrum. Our plan is to explore various approaches to achieve fast reconnection while minimizing the impact on multiple x-line formation. We should be able to correctly capture the physics of the acceleration of suprathermal electrons in a macroscale system with none of the constraints associated with including kinetic-scale boundary layers—there are no kinetic-scale boundary layers in the model. This *kglobal* code is operational, and preliminary tests of its capabilities have been described in the study by Drake *et al.*[12] It correctly describes an Alfvén wave in the presence of a pressure anisotropy and reproduces the linear growth rate of the firehose instability.

The large-scale parallel electric field is obtained by combining the parallel momentum equations for the three species (ions, cold electrons, and hot electrons) into a single equation for the total parallel current. Because of constraints on this current, the driver of the current must be small and therefore can be set to zero, which yields a constraint equation for the parallel electric field. The details of the calculation are shown in the Appendix. The resulting expression for the parallel electric field is given by

$$E_\parallel = \frac{-1}{n_i e}\left(\boldsymbol{B}\cdot\nabla\left(\frac{m_e n_c v_{\parallel c}^2}{B}\right) + \boldsymbol{b}\cdot\nabla P_c + \boldsymbol{b}\cdot\nabla\cdot\boldsymbol{T}_h\right), \quad (1)$$

where m_e is the electron mass, n_c, n_h, $n_i = n_c + n_h$, $v_{\parallel c}$, $v_{\parallel h}$, and $v_{\parallel i}$ are the densities and flow speeds (parallel to the magnetic field) of the two electron species and the ions, respectively, P_c is the scalar pressure of the cold electron fluid, B is the magnetic field, $\boldsymbol{b}$ is a unit vector along $\boldsymbol{B}$, and $\boldsymbol{T}_h$ is the gyrotropic stress tensor of the hot electron particles, including their inertial contributions,[12]

$$\boldsymbol{T}_h = T_{eh\parallel}\boldsymbol{b}\boldsymbol{b} + P_{eh\perp}(\boldsymbol{I} - \boldsymbol{b}\boldsymbol{b}), \quad (2)$$

where $\boldsymbol{I}$ is the unit tensor, $T_{eh\parallel}$ is the stress tensor along the magnetic field $\boldsymbol{B}$, and $P_{eh\perp}$ is the usual perpendicular pressure,

$$P_{eh\perp} = \int d\boldsymbol{p}_e \frac{p_{e\perp}^2}{2m_e\gamma_e}f, \quad (3)$$

where in the frame drifting with $\boldsymbol{v}_E = c\boldsymbol{E}\times\boldsymbol{B}/B^2$, there are no perpendicular flows, and so $f = f(\boldsymbol{x}, p_{e\parallel}, p_{e\perp}, t)$. $T_{eh\parallel}$ includes the mean parallel drifts of the hot electrons,

$$T_{eh\parallel} = \int d\boldsymbol{p}_e \frac{p_{e\parallel}^2}{m_e\gamma_e}f, \quad (4)$$

with $p_{e\parallel}$ being the hot parallel electron momentum with relativistic factor γ_e. The normalizations for *kglobal* described in the study by Drake *et al.*[12] remain unchanged. However, we now have a separate normalization for the parallel electric field, $E_\parallel \sim m_e C_{Ae}^2/eL_0 = m_i C_A^2/eL_0$, where C_{Ae} is the electron Alfvén speed and L_0 is the length scale of the domain. The normalization for $E_\parallel$ comes from parallel force balance. Compared to the usual scaling for the perpendicular electric field $\boldsymbol{E}_\perp \sim C_A B_0/c$, the parallel electric field satisfies $E_\parallel/E_\perp \sim d_i/L_0 \ll 1$. Thus, we only keep the parallel electric field for motion along the field lines and it can therefore be neglected in Faraday's equation when evolving the magnetic field. The addition of this electric field

modifies the momentum equation for the ions and the guiding center equation for the particle electrons from Ref. 12 in the following way:

$$\rho \frac{d\boldsymbol{v}}{dt} = \frac{1}{c}\boldsymbol{J} \times \boldsymbol{B} - \nabla P_i - \nabla_\perp P_c - (\nabla \cdot \boldsymbol{T}_{eh})_\perp + en_iE_\|\boldsymbol{b}$$
$$- m_en_cv_{\|c}^2\boldsymbol{\kappa}, \qquad (5)$$

$$\frac{d}{dt}p_{e\|} = p_{e\|}\boldsymbol{v}_E \cdot \boldsymbol{\kappa} - \frac{\mu_e}{\gamma_e}\boldsymbol{b} \cdot \nabla B - eE_\|, \qquad (6)$$

where $\kappa = \boldsymbol{b} \cdot \nabla \boldsymbol{b}$ is the magnetic curvature and $\mu_e = p_{e\perp}^2/2m_eB$ is the magnetic moment of the electron. Note that in Eq. (5) the gradients of the cold electron pressure and hot electron stress tensor are now in the perpendicular direction only. See the Appendix for a derivation of Eq. (5). Since the parallel electric field is the same order as the pressure terms in Eq. (5), thermal particles are reflected by this electric potential, which prevents heated electrons from escaping from the reconnection diffusion region and the exhaust.[14,25] The consequence for electrons is that they can undergo multiple Fermi reflections within the reconnection exhaust, which facilitates the initial energy gain of electrons.

With the inclusion of a large-scale parallel electric field, *kglobal* should correctly describe the dynamics of hot electrons escaping along the ambient magnetic field in an open system and the development of a return current of cold electrons. The large-scale parallel electric field suppresses the escape of hot electrons and drives a return current of cold electrons. In its most basic form, this dynamics can be reduced to that of an electron acoustic mode, which can exist in plasmas with separate and distinct electron populations.[19] In the electron acoustic mode, the electrons slosh back and forth on a short time scale so that the ions are practically stationary. Thus, we benchmark *kglobal* by simulating this process.

II. TESTING

Since electron acoustic waves only involve electron motion parallel to the magnetic field, the only nonzero gradients are along the magnetic field. Thus, the perturbed distribution function, $\tilde{f}$, of the hot electrons is only a function of $v_\|$ and $x_\|$. We obtain

$$\partial_t\tilde{f} + v_\|\nabla_\|\tilde{f} - \frac{e}{m_e}\tilde{E}_\|\partial_{v_\|}f_0 = 0. \qquad (7)$$

Similarly, by enforcing charge neutrality and taking the cold electron pressure from the constancy of $P_c/n_c^{5/3}$, Eq. (1) becomes

$$\tilde{E}_\| = -\frac{1}{n_ie}\left(\frac{5}{3}\nabla_\|T_c\tilde{n}_h + \nabla_\|\tilde{T}_h\right). \qquad (8)$$

By assuming that the unperturbed hot electron distribution function is a Maxwellian, we can solve Eq. (7) for $\tilde{f}$ and take the moments to obtain the first order corrections to the hot electron density and pressure. After some algebra, the dispersion function for the electron acoustic wave is

$$\frac{n_{0c}}{n_{0h}} = Z'(\zeta)\left(\frac{5}{6}\frac{T_{0c}}{T_{0h}} + \zeta^2\right), \qquad (9)$$

where n_{0c} is the unperturbed density of the cold electrons (fluid), n_{0h} is the unperturbed density of the hot electrons (particles), T_{0c} is the unperturbed temperature of the cold electrons, T_{0h} is the unperturbed

temperature of the hot electrons, $\zeta = \omega/kv_{th}$, v_{th} is the thermal speed of the hot electrons, and $Z'(\zeta)$ is the derivative of the plasma dispersion function. Note that this result matches that of Gary and Tokar[19] in the long wavelength limit $k \ll k_{De}$, where k_{De}^{-1} is the Debye length. For $T_{0c} \ll T_{0h}$ and $n_{0c} \ll n_{0h}$, the phase speed of the wave is small compared to v_{th} and the mode is only weakly damped and has a characteristic frequency,

$$\omega = kv_{th}\sqrt{\frac{n_{0c}}{n_{0h}} + \frac{5}{6}\frac{T_{0c}}{T_{0H}}}. \qquad (10)$$

We numerically solved this equation for various values of the density and temperature ratios and obtained the frequency and decay rates of these waves. For each value of the two parameters, we initialized *kglobal* with a sinusoidal perturbation in the electron density and temperature and measured the corresponding frequencies and decay rates of the resulting disturbance. The results of the linear theory and the simulation results are plotted in Fig. 1. The damping rate of the mode is controlled by the Landau resonance with the energetic component which is accurately captured by the code, a remarkable result. A similar argument can show that *kglobal* can damp ion acoustic waves with Landau damping as well.

In our final test, we compare a simulation with *kglobal* to a simulation with the PIC code p3d.[43] We set up a simplified version of what we expect to see in a reconnection exhaust. The initial conditions consist of a constant magnetic field, a constant density made up of 75% particle electrons and 25% fluid electrons, and a temperature profile for the particle electrons that increases sharply in the center to twenty times the asymptotic value as can be seen in Fig. 2(a). This value of the hot to cold electron density ratio was chosen to quicken the dynamics since we know from Fig. 1(b) that the larger the ratio the larger the damping rate. To convert this setup to a PIC version, we had to make sure that the smallest length scale in *kglobal* was much larger than the Debye length since this scale is not resolved in *kglobal*. Thus, we
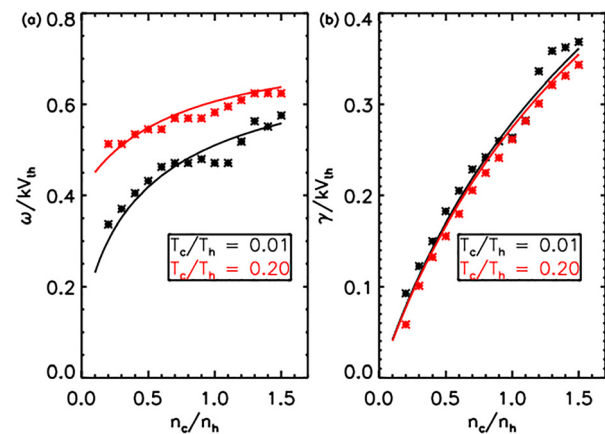

FIG. 1. In panel (a), the electron acoustic wave phase speed vs the cold to hot density ratio of the electrons. In panel (b), the electron acoustic wave damping rate vs the cold to hot density ratio of the electrons. The stars are taken from the simulations and the lines are from the linear theory. Note that the phase speed is normalized to the thermal speed of the hot electrons and the damping rate is normalized to the time a thermal particle requires to travel one wavelength.
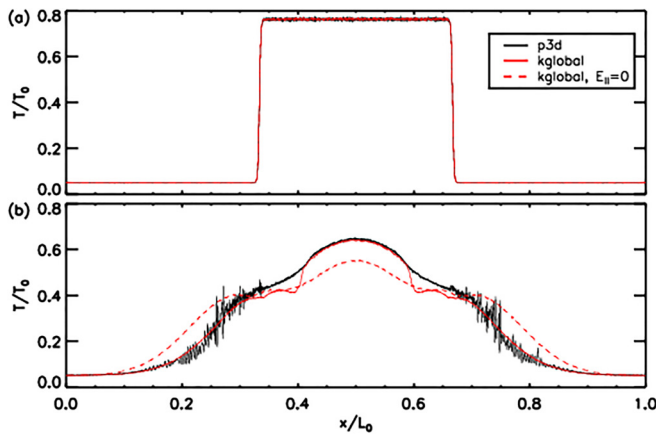
FIG. 2. Profiles of the total electron temperature for the PIC code *p3d* (black), the *kglobal* code with the included parallel electric field (red) and without the parallel electric field (dashed red). In panel (a), at $t/t_{th} = 0$. In panel (b), at $t/t_{th} = 0.12$ where t_{th} is the time a hot thermal electron requires to travel the length of the box.

FIG. 3. The log of the particle distribution functions from the PIC code *p3d* (black) and the *kglobal* code (red) taken at $x/L_0 = 0.25$. Notice the dip in the *kglobal* distribution function around $v/C_A = -30$.

equated the transition width between the two regions of hot and cold electrons to 30 times the Debye length.

In both the simulations, we utilized a large spatial domain in the parallel direction, and so there is space for the hot electrons to expand. A small domain in the perpendicular direction was included so that the data could be averaged over this direction to decrease particle noise. For *kglobal*, we had a domain of 2048×64 cells and for *p3d*, 8192×64. In both simulations, the electron to ion mass ratio was 1/1836 and the speed of light was 300 times the Alfvén speed. For *p3d*, a uniform background with a constant density and a temperature corresponding to the cold electron fluid in *kglobal* was included along with an electron population with the same temperature profile as the hot species in *kglobal*. The results from these simulations are shown in Fig. 2. The PIC simulation is in solid black, *kglobal* is in red, and the result from *kglobal* without a parallel electric field is in dashed red. We added the latter, and so we could determine how the addition of the parallel electric field influenced the dynamics. First, the temperature profiles from *p3d* and *kglobal* with $E_\parallel$ match very well over most of the domain. In contrast, the temperature in *kglobal* with $E_\parallel = 0$ spreads much more rapidly, demonstrating that $E_\parallel$ does inhibit electron thermal transport and that the model for $E_\parallel$ in *kglobal* correctly describes transport suppression.

While *kglobal* is able to capture the overall dynamics of the temperature profile, it does not produce the short scale spatial oscillations seen in the *p3d* data. These oscillations are plasma waves driven unstable by a bump-on-tail velocity distribution that smooths out the plateaus in the temperature visible in the *kglobal* data around 0.3 $< x/L_0 < 0.4$ and $0.6 < x/L_0 < 0.7$. Figure 3 displays the distribution functions from *p3d* in black and from *kglobal* in red at $x/L_0 = 0.25$ at the time shown in panel (b) of Fig. 2. Note that for *kglobal*, a Maxwellian with density and temperature equal to that of the cold electron fluid was added to the hot electron distribution function so that we could directly compare cuts with *p3d*. There is a sharp dip visible in the velocity distribution from *kglobal* around $v/C_A = -30$ that is not seen in the data from *p3d*. In the *p3d* simulation, the faster particles have lost energy to plasma oscillations and filled in this dip,
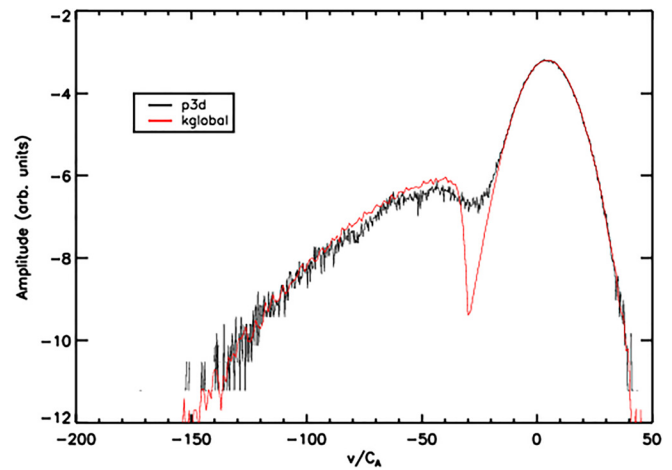
forming a plateau in phase space. This result is not seen in the *kglobal* data because this model does not support plasma waves, which require a violation of charge neutrality to exist. Electron sound waves can be driven unstable by structures in velocity space, but the phase speed of these waves is fixed by the local plasma parameters [see Eq. (9)] and so will typically not be resonant with electrons in the bump region shown in Fig. 3.

III. CONCLUSION

The *kglobal* code[12] has been upgraded to include a macroscale $E_\parallel$ that develops as a result of gradients in the plasma pressure parallel to the ambient magnetic field. The upgraded model now captures the dynamics of electron acoustic waves and accurately describes the suppression of transport of hot electrons parallel to the ambient magnetic field, a process that is important in the early phases of electron acceleration in magnetic reconnection.[15,25] The inclusion of the large scale $E_\parallel$ is also important in describing the development of return currents that form as the hot electrons escape from regions of electron acceleration in macroscale energy release events such as flares in the solar corona. This new capability combined with the ability of the model to describe the impact of pressure anisotropy on magnetic field dynamics (e.g., firehose instability), which is critical for describing the feedback of energetic particles on reconnection dynamics, suggests that the *kglobal* code can be used to accurately simulate nonthermal electron acceleration during magnetic reconnection.

Our next step is to begin to explore the energization of electrons during magnetic reconnection with *kglobal* and to determine whether the reconnection dynamics in a macroscale system can produce power law distributions that are ubiquitous in observations.[20,33] Because *kglobal* is a macroscale model, the dynamics of particle acceleration can be explored in a much larger domain than with a traditional PIC model. In addition, we will include particle loss in a realistic manner to establish whether or not it is the balance between the reconnection drive and the escape of energetic particles that leads to power law distributions.[11,23] Finally, in a macroscale simulation model, the

inclusion of a synthetic diagnostic to describe synchrotron emission and bremsstrahlung emission will be possible.

ACKNOWLEDGMENTS

APPENDIX: ENERGY CONSERVATION

We start with the momentum equations for the three species, the ions

$$\rho \frac{d\boldsymbol{v}_i}{dt} = ne\boldsymbol{E} + \frac{ne}{c}\boldsymbol{v}_i \times \boldsymbol{B} - \nabla P_i, \tag{A1}$$

the cold electrons

$$\frac{\partial(m_e n_c v_{\|c}\boldsymbol{b})}{\partial t} = -n_c e\boldsymbol{E} - \frac{n_c e}{c}\boldsymbol{v}_c \times \boldsymbol{B} - \nabla P_c$$
$$-\boldsymbol{b}\boldsymbol{B}\cdot\nabla\frac{m_e n_c v_{\|c}^2}{B} - m_e n_c v_{\|c}^2\boldsymbol{\kappa}, \tag{A2}$$

and the hot electrons

$$\frac{\partial(m_e n_h \bar{v}_{\|h}\boldsymbol{b})}{\partial t} = -n_h e\boldsymbol{E} - \frac{n_h e}{c}\bar{\boldsymbol{v}}_h \times \boldsymbol{B} - \nabla\cdot\boldsymbol{T}_h, \tag{A3}$$

where ρ and $\boldsymbol{v}$ are the ion mass density and velocity, from charge neutrality $n = n_c + n_h$ and the electron inertia has only been retained in the direction along the ambient magnetic field. In writing the electron momentum equations, we have for simplicity assumed that the mean drifts of both species are not relativistic. The individual electron fluxes can be of order nc_{Ae}, while the ion flux is of order nc_A. However, we show below that the total current is much smaller than the contribution from each species of particle and this yields a constraint on the total driver of the current. To see this, we divide the momentum equations along the field lines by their respective masses and subtract Eqs. (A2) and (A3) from Eq. (A1), which yields

$$\frac{1}{e}\frac{\partial J_{\|}}{\partial t} = \frac{n_i e E_{\|}}{m_e} - \boldsymbol{b}\cdot\left(\frac{1}{m_e}\nabla P_c + \frac{1}{m_e}\nabla\cdot\boldsymbol{T}_h\right)$$
$$-\boldsymbol{B}\cdot\nabla\left(\frac{n_c v_{\|c}^2}{B}\right). \tag{A4}$$

All of the terms on the right-hand side of this equation act as drivers of $J_{\|}$. However, the parallel current driven is constrained by the structure of the magnetic field which is produced by this current. This constraint follows from Ampère's law $J_{\|} \sim cB/4\pi L$, where L is

the macroscopic characteristic perpendicular scale of the magnetic field. Comparing the time derivative of this current, given by c_A/L, with the characteristic scaling of the terms on the right, e.g., the gradient of the hot thermal electrons, which scales as $n_h T_h/m_e L$, we find that the ratio of the left to the right side of the equation scales like $\sqrt{m_e/m_i}(d_e/L) \ll 1$. Thus, the time derivative of the current can be discarded. This tells us that

$$v_{\|c} = \frac{1}{n_c}(n_i v_{\|i} - n_h v_{\|h}). \tag{A5}$$

Note that this constraint equation for $v_{\|c}$ includes the ion motion. That the ions must also be included in the constraint follows because the mean drift speed associated with the current (from the previous scaling for $J_{\|}$) scales like $nc_A(d_i/L) \ll nc_A$, the characteristic current carried by the ions. This constraint on the parallel flows is consistent with the conclusions of Kulsrud[29] and yields the equation for $E_{\|}$ in Eq. (1). If the mean flows of the electrons become relativistic, corrections to Eq. (1) of order $v_{\|h}/c$ must be included.

A further consequence of this result is that the sum of the fluxes of the two electron species is limited to a scale of the order of the ion flux. The consequence is that when the three-momentum equations are summed, the electron inertia arising from the time derivative can be discarded, which yields the ion momentum equation

$$\rho \frac{d\boldsymbol{v}}{dt} = \frac{1}{c}\boldsymbol{J} \times \boldsymbol{B} - \nabla(P_i + P_c) - \nabla\cdot\boldsymbol{T}_{eh} - \boldsymbol{b}\boldsymbol{B}\cdot\nabla\frac{m_e n_c v_{\|c}^2}{B}$$
$$-m_e n_c v_{\|c}^2\boldsymbol{\kappa}, \tag{A6}$$

which is equivalent to the form shown in Eq. (5). To explore energy conservation of Eqs. (5) and (6) along with the usual fluid equations, we take the dot product of Eq. (5) with $\boldsymbol{v}$ and use the ion continuity equation to obtain

$$\frac{\partial}{\partial t}\frac{\rho v^2}{2} + \nabla\cdot\frac{\rho\boldsymbol{v}v^2}{2} + \boldsymbol{v}\cdot\nabla P_i$$
$$= (\boldsymbol{J}_{\perp} - \boldsymbol{J}_{\perp c} - \boldsymbol{J}_{\perp h})\cdot\boldsymbol{E}_{\perp} - (J_{\|c} + J_{\|h})E_{\|}$$
$$= \boldsymbol{J}_{\perp}\cdot\boldsymbol{E}_{\perp} - (\boldsymbol{J}_c + \boldsymbol{J}_h)\cdot\boldsymbol{E}, \tag{A7}$$

where we have used the perpendicular components of Ohm's law $\boldsymbol{E}_{\perp} = -\boldsymbol{v}\times\boldsymbol{B}/c$, the perpendicular components of the two electron momentum equations, and Eq. (A5) for $v_{\|c}$. From Faraday's law, we find

$$\frac{\partial}{\partial t}\frac{B^2}{8\pi} + \frac{c}{4\pi}\nabla\cdot(\boldsymbol{E}\times\boldsymbol{B}) + \boldsymbol{J}_{\perp}\cdot\boldsymbol{E}_{\perp} = 0, \tag{A8}$$

which, when combined with Eq. (A7), yields the conservation law

$$W_{MHD} + W_c + W_h = constant, \tag{A9}$$

where we have discarded terms corresponding to the divergence of the various energy fluxes. The MHD energy, W_{MHD}, includes the ion bulk kinetic and thermal energies and the magnetic energy, and the cold electron energy includes both the kinetic energy associated with parallel streaming and the thermal energy

$$W_c = \frac{m_e n_c v_{\|c}^2}{2} + \frac{1}{\Gamma - 1}P_c, \tag{A10}$$

with Γ being the ratio of specific heats. The hot electron energy is the sum of the parallel kinetic energies of all hot electrons as well as the energy associated with their perpendicular gyro motion. It does not include the kinetic energy associated with the perpendicular bulk flow, which is negligible.

REFERENCES

[1]E. P. Alves, J. Zrake, and F. Fiuza, "Efficient nonthermal particle acceleration by the kink instability in relativistic jets," Phys. Rev. Lett. **121**, 245101 (2018).

[2]D. Ball, L. Sironi, and F. Özel, "Electron and proton acceleration in trans-relativistic magnetic reconnection: Dependence on plasma beta and magnetization," Astrophys. J. **862**, 80 (2018).

[3]J. T. Dahlin, J. F. Drake, and M. Swisdak, "The mechanisms of electron heating and acceleration during magnetic reconnection," Phys. Plasmas **21**, 092304 (2014).

[4]J. T. Dahlin, J. F. Drake, and M. Swisdak, "Electron acceleration in three-dimensional magnetic reconnection with a guide field," Phys. Plasmas **22**, 100704 (2015).

[5]J. T. Dahlin, J. F. Drake, and M. Swisdak, "Parallel electric fields are inefficient drivers of energetic electrons in magnetic reconnection," Phys. Plasmas **23**, 120704 (2016).

[6]J. T. Dahlin, J. F. Drake, and M. Swisdak, "The role of three-dimensional transport in driving enhanced electron acceleration during magnetic reconnection," Phys. Plasmas **24**, 092110 (2017).

[7]W. Daughton, V. Roytershteyn, H. Karimabadi, L. Yin, B. J. Albright, B. Bergen, and K. J. Bowers, "Role of electron physics in the development of turbulent magnetic reconnection in collisionless plasmas," Nat. Phys. **7**, 539–542 (2011).

[8]J. F. Drake, M. A. Shay, W. Thongthai, and M. Swisdak, "Production of energetic electrons during magnetic reconnection," Phys. Rev. Lett. **94**, 095001 (2005).

[9]J. F. Drake, M. Swisdak, M. K. Schoeffler, B. N. Roger, and S. Kobayashi, "Formation of secondary islands during magnetic reconnection," Geophys. Res. Lett. **33**, L13105, https://doi.org/10.1029/2006GL025957 (2006).

[10]J. F. Drake, M. Swisdak, H. Che, and M. Shay, "Electron acceleration from contracting magnetic islands during reconnection," Nature **443**, 553–556 (2006).

[11]J. F. Drake, M. Swisdak, and R. Fermo, "The power-law spectra of energetic particles during multi-island magnetic reconnection," Astrophys. J., Lett. **763**, L5 (2013).

[12]J. F. Drake, H. Arnold, M. Swisdak, and J. T. Dahlin, "A computational model for exploring particle acceleration during reconnection in macroscale systems," Phys. Plasmas **26**, 012901 (2019).

[13]J. Egedal, W. Fox, N. Katz, M. Porkolab, M. Øieroset, R. P. Lin, W. Daughton, and J. F. Drake, "Evidence and theory for trapped electrons in guide field magnetotail reconnection," J. Geophys. Res. **113**, A12207, https://doi.org/10.1029/2008JA013520 (2008).

[14]J. Egedal, W. Daughton, and A. Le, "Large-scale electron acceleration by parallel electric fields during magnetic reconnection," Nat. Phys. **8**, 321–324 (2012).

[15]J. Egedal, W. Daughton, A. Le, and A. L. Borg, "Double layer electric fields aiding the production of energetic flat-top distributions and superthermal electrons within magnetic reconnection exhausts," Phys. Plasmas **22**, 101208 (2015).

[16]A. G. Emslie, H. Kucharek, B. R. Dennis, N. Gopalswamy, G. D. Holman, G. H. Share et al., "Energy partition in two solar flare/CME events," J. Geophys. Res. **109**, A10104, https://doi.org/10.1029/2004JA010571 (2004).

[17]A. G. Emslie, B. R. Dennis, G. D. Holman, H. S. Hudson et al., "Refinements to flare energy estimates: A followup to 'Energy partition in two solar flare/CME events' by A. G. Emslie et al.," J. Geophys. Res. **110**, A11103, https://doi.org/10.1029/2005JA011305 (2005).

[18]A. G. Emslie, B. R. Dennis, A. Y. Shih, P. C. Chamberline, R. A. Mewaldt, and C. S. Moore, "Global energetics of thirty-eight large solar eruptive events," Astrophys. J. **759**, 71 (2012).

[19]S. Gary and R. Tokar, "The electron-acoustic mode," Phys. Fluids **28**, 2439 (1985).

[20]D. E. Gary, B. Chen, B. R. Dennis, G. D. Fleishman, G. J. Hurford, and S. Krucker, "Microwave and hard X-ray observations of the 2017 September 10 solar limb flare," Astrophys. J. **863**, 83 (2018).

[21]M. Gordovskyy, P. Browning, and R. Pinto, "Combining MHD and kinetic modelling of solar flares," Adv. Space Res. **63**, 1453–1465 (2019).

[22]S. E. Guidoni, C. R. DeVore, J. T. Karpen, and B. J. Lynch, "Magnetic-island contraction and particle acceleration in simulated eruptive solar flares," Astrophys. J. **820**, 60 (2016).

[23]F. Guo, H. Li, W. Daughton, and Y. Liu, "Formation of hard power laws in the energetic particle spectra resulting from relativistic magnetic reconnection," Astrophys. J., Lett. **879**, L23 (2014).

[24]F. Guo, X. Li, W. Daughton, P. Kilian, H. Li, Y. Liu, W. Yan, and D. Ma, "Determining the dominant acceleration mechanism during relativistic magnetic reconnection in large-scale systems," Astrophys. J., Lett. **879**, L23 (2019).

[25]C. C. Haggerty, M. A. Shay, J. F. Drake, T. D. Phan, and C. T. McHugh, "The competition of electron and ion heating during magnetic reconnection," Geophys. Res. Lett. **42**, 9657–9665, https://doi.org/10.1002/2015GL065961 (2015).

[26]D. Heristchi and T. Amari, "Solar flare high-energy electron spectra," Sol. Phys. **142**, 209–211 (1992).

[27]S. Krucker, H. S. Hudson, L. Glesener, S. M. White, S. Masuda, J.-P. Wuelser, and R. P. Lin, "Measurements of the coronal acceleration region of a solar flare," Astrophys. J. **714**, 1108–1119 (2010).

[28]S. Krucker and M. Battaglia, "Particle densities within the acceleration region of a solar flare," Astrophys. J. **780**, 107 (2014).

[29]R. M. Kulsrud, "Handbook Plasma Physics," in *MHD Description of Plasma: Basic Plasma Physics* (North-Holland Publishing Company, 1983), Vol. 1, pp. 115–144.

[30]X. Li, F. Guo, H. Li, and G. Li, "Particle acceleration during magnetic reconnection in a low-β plasma," Astrophys. J., Lett. **843**, 1 (2017).

[31]X. Li, F. Guo, H. Li, and S. Li, "Large-scale compression acceleration during magnetic reconnection in a low-β plasma," Sol. Phys. **17**, 412–435 (2018).

[32]R. P. Lin and H. S. Hudson, "10–100 keV electron acceleration and emission from solar flares," Sol. Phys. **17**, 412–435 (1971).

[33]R. P. Lin, S. Krucker, G. J. Hurford, D. M. Smith, H. S. Hudson, and G. D. Holman, "RHESSI observations of particle acceleration and energy release in an intense solar gamma-ray line flare," Astrophys. J. **595**, L69–L76 (2003).

[34]Y. Lin and L. C. Lee, "Structure of the dayside reconnection layer in resistive MHD and hybrid models," J. Geophys. Res.: Space Phys. **98**, A3, https://doi.org/10.1029/92JA02363 (1993).

[35]Y. Liu, M. Hess, F. Guo, W. Daughton, H. Li, P. Cassak, and M. Shay, "Why does steady-state magnetic reconnection have a maximum local rate of order 0.1?," Phys. Rev. Lett. **118**, 085101 (2017).

[36]J. A. Miller, P. J. Cargill, A. G. Emslie, G. D. Holman, B. R. Dennis, and T. N. LaRosa, "Critical issues for understanding particle acceleration in impulsive solar flares," J. Geophys. Res. **102**, 14631–14659, https://doi.org/10.1029/97JA00976 (1997).

[37]M. Øieroset, R. P. Lin, T. D. Phan, D. E. Larson, and S. D. Bale, "Evidence for electron acceleration up to 300 keV in the magnetic reconnection diffusion region of Earth's magnetotail," Phys. Rev. Lett. **89**, 195001 (2002).

[38]M. Oka, S. Ishikawa, P. Saint-Hilaire, S. Krucker, and R. P. Lin, "Kappa distribution model for hard x-ray coronal sources of solar flares," Astrophys. J. **764**, 6 (2013).

[39]P. L. Pritchett and F. V. Coroniti, "Three-dimensional collisionless magnetic reconnection in the presence of a guide field," J. Geophys. Res. **109**, A01220, https://doi.org/10.1029/2003JA009999 (2004).

[40]M. Shay, J. F. Drake, and M. Swisdak, "Two-scale structure of the electron dissipation region during collisionless magnetic reconnection," Phys. Rev. Lett. **99**, 155002 (2007).

[41]D. A. Uzdensky, N. F. Loureiro, and A. A. Schekochihin, "Fast magnetic reconnection in the plasmoid-dominated regime," Phys. Rev. Lett. **105**, 235002 (2010).

[42]H. Wang, Q. Lu, C. Huang, and S. Wang, "The mechanisms of electron acceleration during multiple X line magnetic reconnection with a guide field," Astrophys. J. **821**(2), 84 (2016).

[43]A. Zeiler, D. Biskamp, J. F. Drake, B. N. Rogers, M. A. Shay, and M. Scholer, "Three-dimensional particle simulations of collisionless magnetic reconnection," J. Geophys. Res. **107**, 1–9, https://doi.org/10.1029/2001JA000287 (2002).